DESIGNED MONOMERS AND POLYMERS
2024, VOL. 27, NO. 1, 1–20
https://doi.org/10.1080/15685551.2024.2352897

Taylor & Francis
Taylor & Francis Group

A new polyazomethine-based pyrazole moiety and its reinforced nanocomposites @ ZnO for antimicrobial applications

Aqilah A. Hakami[a], Hajar S. Alorfi[a], Thoraya A. Farghaly[b,c] and Mahmoud A. Hussein[a,d]

[a]Chemistry Department, Faculty of Science, King Abdulaziz University, Jeddah, Saudi Arabia; [b]Department of Chemistry, Faculty of Science, Cairo University, Giza, Egypt; [c]Department of Chemistry, Faculty of Applied Science, Umm Al-Qura University, Makkah Almukkarramah, Saudi Arabia; [d]Chemistry Department, Faculty of Science, Assiut University, Assiut, Egypt

ABSTRACT

A new class of biologically active polyazomethine/pyrazole and their related nanocomposites, polyazomethine/pyrazole/zinc oxide nanoparticles, have been successfully synthesized through the polycondensation technique in the form of polyazomethine pyrazole ($PAZm/Py_{4–6}$) and polyazomethine/pyrazole/zinc oxide nanoparticles ($PAZm/Py/ZnO_{a-c}$). The polymeric nanocomposites were prepared with a 5% loading of zinc oxide nanofiller using the same preparation technique, in addition to the help of ultrasonic radiation. The characteristics of the new polymers, such as solubility, viscometry, and molecular weight, were examined. All the polymers were completely soluble in the following solvents: concentrated sulfuric acid, formic acid, dimethylformamide, dimethyl sulfoxide, and tetrahydrofuran. Furthermore, the weight loss of the polyazomethine pyrazole (4, 5, and 6) at 800 °C was 67%, 95%, and 86%, respectively, which indicates the thermal stability of these polymers. At 800 °C, the polyazomethine/pyrazole/zinc oxide nanoparticles (a, b, and c) lost 74%, 68%, and 75% of their weight, respectively. This shows that adding zinc oxide nanoparticles made these compounds more stable at high temperatures. The X-Ray diffraction pattern of the polyazomethine pyrazole ($PAZm/Py_{4–6}$) shows a number of sharp peaks with varying intensities. The polymers that were studied had straight crystal structures. Furthermore, the measurements of polyazomethine/pyrazole/zinc oxide nanoparticles ($PAZm/Py/ZnO_{a-c}$) indicate a good merging of zinc oxide nanoparticles into the matrix of polymers. The antimicrobial activity of polymers and polymer nanocomposites was tested against some selected bacteria and fungi. The synthesized polymer (c) shows the highest activity against the two types of gram-negative bacteria selected. Most tested compounds were found to be effective against gram-positive bacteria except polyazomethine pyrazole ($PAZm/Py_5$) and polyazomethine pyrazole ($PAZm/Py_6$), which do not exhibit any activity. The synthesized polymers and their related nanocomposites were tested for their ability to kill the chosen fungi. All of them were effective against Aspergillus flavus, but only polyazomethine pyrazole ($PAZm/Py_4$) and polyazomethine/pyrazole/zinc oxide ($PAZm/Py/ZnO_c$) were effective against Candida albicans.

ARTICLE HISTORY
Received 9 October 2023
Accepted 4 May 2024

KEYWORDS
Nanocomposites; biologically interest; polyazomethine; pyrazole; Zinc oxide NPs

1. Introduction

The synthesis of new polymers with interesting properties biologically, thermally, mechanically, and others has attracted a lot of attention. Polyazomethines are one of the π-conjugated polymers that have the ability to complex and protonate and are distinguished by the presence of HC=N in their design. It was first prepared in 1923 by Adams and his group [1]. They are also called Schiff base polymers or polyimines. This polymer's thermal stability, nonlinear optical, electronic, optoelectronic, and liquid crystalline properties characterize this polymer, making it interesting in the science of materials [2–7]. Schiff bases are compounds that have a variety of uses in a range of fields as diverse as farming, cosmetics, and medicine, and these compounds have antitumor, antibacterial, and anticancer activity [8–13]. The polymers made of polyazomethines have disadvantages like a high melting point, poor solubility in most organic solvents, and a tendency to form mesophases when heated [14]. These defects limit processability. Therefore, various methods were used to facilitate the polyazomethines' processability, including adding different substituted benzene rings into the main chain, and various types of heterocyclic units were used in monomers [15–18]. One of the most promising areas of current research and development is polymer nanocomposites. Recent attention has been drawn to metal oxide nanoparticles of zinc, copper, iron, and cerium oxide because of their distinctive physical,

CONTACT Mahmoud A. Hussein mahussein74@yahoo.com; maabdo@kau.edu.sa Chemistry Department, Faculty of Science, King Abdulaziz University, P.O. Box 80203, Jeddah 21589, Saudi Arabia

chemical, and biological properties [19–21]. Zinc oxide nanoparticles (ZnO NPs), which are among these metal oxide nanoparticles, are frequently chosen because of their nontoxicity and are used in many different fields [22–34]. Gram-positive and Gram-negative bacteria are the causes of numerous human diseases, and these bacteria are evolving resistance to commercial antibiotics, phytoncides, and traditional natural remedies [35]. Developing bacterial resistance to common antibiotics has become a serious problem for the biopharmaceutical sector and for public health [36]. Therefore, the creation of novel biocidal agents to combat bacterial pathogens that are multi-drug resistant is urgently needed. Recently, ZnO NPs have demonstrated the effectiveness of eliminating bacterial pathogens, fungal, and cancer cells in a cost-effective and environmentally friendly manner [22,37–45]. The objective of this work was to synthesize and characterize some new hetero-aromatic polyazomethine polymers and their related ZnO nanocomposites through the polycondensation technique. One of the advantages of this method is its ease of application. It is not harmful to the environment since water is used as a medium. Special attention will be given to the pyrazole moiety as one of the most interesting biologically applicable moieties a long time ago [46–58]. The characteristics of the new polymers, such as solubility, viscometry, and molecular weight, were examined. Furthermore, the polymers and polymer nanocomposites produced were identified using Fourier transform infrared (FT-IR) spectroscopy and characterized using standard characterization tools such as X-ray diffraction (XRD), scanning electron microscopy (SEM), and transmission electron microscopy (TEM). Thermal behavior of compounds, such as thermogravimetric analysis (TGA) and derivative thermogravimetric (DTG) analysis, was also discussed. The antimicrobial activities of newly synthesized polymers and polymer nanocomposites against various bacterial and fungal species were evaluated.

2. Experimental section

2.1. Materials

Substituted aniline derivatives (2-chloroaniline, 3-chloroaniline, 4-chloroaniline) were purchased from (PDH, Germany) and used as starting materials for the synthesis of monomers. Sodium nitrite ($NaNO_2$), malononitrile ($CH_2(CN)_2$), sodium acetate ($C_2H_3NaO_2$), and hydrazine hydrate were purchased from (Sigma-Aldrich, U.S.A.) and used directly as it was received. Zinc oxide NPs were supplied by NANO TECH Co. LTD Egypt and used to fabricate polymers nanocomposites. Glacial acetic acid CH_3CO_2H (99%) from Sigma-Aldrich was used as a catalyst. Terephthalaldehyde purchased from NANO TECH Co. LTD Egypt. concentrated hydrochloric acid (HCl) was received from (Merck, Germany), as a solvent with a purity of (99%) was used for dissolving substituted aniline derivatives. Ethanol absolute (99.9% pure) provided by (PDH, Germany) was used as solvent in the monomers, polymers, and polymer nanocomposites synthesis. All of the chemicals and solvents mentioned were used without any more purification because they were all highly pure.

2.2. Instruments and measurements

To characterize and study the applications of the new synthesis polymers the following instruments were used as follows:

Fourier Transform Infrared (FT-IR) spectrophotometer technique is used to analyze the functional groups present in final products, the (Perkin Elmer Precisely Spectrum 100) was used to record the infrared spectra. Each spectrum was in the 400–4000 cm^{-1} wavenumber range. The ^1H NMR spectra of the new polymers were obtained in using a Brucker ASCEND 850 MHz CRYO PROBE 4 CHANNELS 1 H. The samples dissolved in deuterated Dimethyl sulfoxide DMSO-d6 Chemical shifts were related to that of the solvent. The X-Ray Diffraction (XRD) is a technique used to determine whether a material is crystalline or amorphous. The XRD of polymers was recorded using (XRD) D8 ADVANCE in the range 2θ between 5° and 80° at 40 kV voltage and 40 mA using Cu-Kα radiation. Scanning Electron Microscope (JSM-7610FPlus Schottky Field Emission) was used to know Surface morphology of materials. The thermal behavior of all polymers and polymer nanocomposites were evaluated by a Thermo-Gravimetric Analysis (TGA) and derivative thermal gravimetric (DTG) using a Shimadzu TG-50 H thermal analyzer at temperatures rising from air temp to 800 °C and heating rate of 10 °C/min. Agilent-GPC Agilent Technologies in Germany was used to determine the molecular weight of the new polyazomethine polymers. G-1362A was the refractive index detector with 100-104-105 A° Altra-styragel columns connected in series. The eluent was THF at a flow rate of 1 mL min^{-1} and in the presence of reference polymer (PS polystyrene). The GPC equipment was run under the following situations: flow rate = 2.000 mL min^{-1}, injection volume = 100.000 µL, and sample concentration = 1.000 g L^{-1}.

2.3. Synthesis of PAZm/Py$_{4-6}$ polymers

2.3.1. Monomer synthesis

The monomers were synthesized according to the following general procedure [59–61]:

In a suitable beaker, 0.01 mole of substituted aniline derivatives **1d-f** were mixed with 10 ml concentrated hydrochloric acid (HCl) to dissolve, then the solutions were left to cool to 0–5 ºC in an ice bath. In another beaker, 0.01 mole of sodium nitrite ($NaNO_2$) was dissolved in 3 ml of water. To form the diazonium salts of aniline derivatives the sodium nitrite solution was added dropwise to the solutions of aniline hydrochloride derivatives with continuous stirring (in an ice bath). In the presence of 0.01 mole of sodium acetate, the clear solutions of substituted diazonium salts were then added dropwise to solutions of 0.01 mole of malononitrile in 20 ml of ethanol. The solutions were stirred for a further 4 h in an ice bath, then colored. The solid products were collected, and washed with cold water and crystallized from ethanol to give the derivatives **4d-f**. The latter derivatives were cyclized as follow: To a solution of derivatives **4d-f** (0.01mole) in ethanol (30 ml), hydrazine hydrate (0.5 g, 0.01 mole) was added and the whole solutions were refluxed for 5 h. After the reactions were completed through investigation with TLC test, the solid precipitated products were collected with filtration and crystallized from ethanol to afford the diaminopyrazole derivatives **5d-f**.

2.3.1.1. Synthesis of 4-((4-chlorophenyl) diazenyl)-1 H-pyrazole-3,5-diamine (d). The monomer (d) was prepared using the aniline derivative (4-chloroaniline) in the same way as the previous preparation, yielding (90%) as a yellow crystals, m.p. 267–270 °C. FT-IR: 3400–3100 cm^{-1} [NH, NH_2 (3-NH_2 and 5-NH_2)], 1451 cm^{-1} (N=N), 1604 cm^{-1} (C=N), 3050–3010 cm^{-1} (=C-H aromatic), 1543 cm^{-1} and 1410 cm^{-1} (C=C). 821 cm^{-1} (C-Cl).

2.3.1.2. Synthesis of 4-((2-chlorophenyl) diazenyl)-1 H-pyrazole-3,5-diamine (e). The monomer (**e**) was prepared using the aniline derivative (2-chloroaniline) in the same way as the previous preparation, yielding (90%) as a yellow crystals, m.p. 267–270 °C. FT-IR: 3400–3100 cm^{-1} [NH, NH_2 (3-NH_2 and 5-NH_2)], 1607 cm^{-1} (C=N), 3050–3010 cm^{-1} (=C-H aromatic), 1544 cm^{-1} and 1458 cm^{-1} (C=C). 1460 cm^{-1} (N=N), 750 cm^{-1} (C-Cl).

2.3.1.3. Synthesis of 4-((3-chlorophenyl) diazenyl)-1 H-pyrazole-3,5-diamine (f). The monomer (**f**) was prepared using the aniline derivative (3-chloroaniline) in the same way as the previous preparation, yielding (90%) as a yellow crystals, m.p. 267–270 °C. FT-IR: 3400–3100 cm^{-1} [NH, NH_2 (3-NH_2 and 5-NH_2)], 1611 cm^{-1} (C=N), 3050–3010 cm^{-1} (=C-H aromatic), 1560 cm^{-1} and 1469 cm^{-1} (C=C). 1428 cm^{-1} (N=N), 786 cm^{-1} (C-Cl).

2.3.2. Polymer synthesis

A mixture of terephthalaldehyde suspended in ethanol, a few drops of glacial acetic acid, and diaminopyrazole derivatives 5d-f dissolved in ethanol were added in a three-necked flask equipped with a condenser, dry nitrogen, and magnetic stir bar. At about 70–80°C, the stirring was continued for 8 h. Then by filtration, the polymer precipitated was isolated and it was washed with hot ethanol and left to dry at room temperature.

2.3.2.1. PAZm/Py$_4$. PAZm/Py_4 was obtained by the polymerization of 1 mole of monomer **d** (0.78 g) with terephthalaldehyde (0.44 g) for 8 h. The polymer yield was 0.92 g (82%) as orange powder. FT-IR: 1627 cm^{-1} (C=N), 2883 cm^{-1} (=C-H stretching of aliphatic), 3263 cm^{-1} (N-H of pyrazole), 1480 cm^{-1} and 1602 cm^{-1} (C=C of the aromatic), 3050 cm^{-1} (C-H stretching of aromatic), 825 cm^{-1} (C-Cl). ^{1}H-NMR (DMSO-d6): δ10.2–10.6 (ss, 2 H, CH=N), δ 12.8 (s, 1 H, N-H), δ 7.14–9.75 (8 H, aromatic protons overlapped).

2.3.2.2. PAZm/Py$_5$. PAZm/Py_5 was obtained by the polymerization of 1 mole of monomer **e** (1.18 g) with 1 mole of terephthalaldehyde (0.67 g) for 8 h. The polymer yield was 1.42 g (85%) as red powder. FT-IR: 1634 cm^{-1} (C=N), 2889 cm^{-1} (=C-H stretching of aliphatic), 3274 cm^{-1} (N-H of pyrazole), 1456 cm^{-1} and 1602 cm^{-1} (C=C of the aromatic), 3051 cm^{-1} (C-H stretching of aromatic), 737 cm^{-1} (C-Cl). ^{1}H-NMR (DMSO-d6): δ10–10.5 (ss, 2 H, CH=N), δ 12.4 (s, 1 H, N-H), δ 7.10–9.46 (8 H, aromatic protons overlapped).

2.3.2.3. PAZm/Py$_6$. PAZm/Py_6 was obtained by the polymerization of 1 mole of monomer **f** (1.18 g) with 1 mole of terephthalaldehyde (0.67 g) for 8 h. The polymer yield was 1.17 g (70%) as orange powder. FT-IR: 1630 cm^{-1} (C=N), 2889 cm^{-1} (=C-H stretching of aliphatic), 3284 cm^{-1} (N-H of pyrazole), 1467 cm^{-1} and 1605 cm^{-1} (C=C of the aromatic), 3051 cm^{-1} (C-H stretching of aromatic), 773 cm^{-1} (C-Cl). ^{1}H-NMR (DMSO-d6): δ10.1–10.3 (ss, 2 H, CH=N), δ 12.2 (s, 1 H, N-H), δ 7.19–9.85 (8 H, aromatic protons overlapped).

Table 1. Polymer nanocomposites codes and reaction mixture.

Code	ZnONPs (%)	Reaction mixture
PAZm/Py/ZnO_a	5	4-((2-chlorophenyl) diazenyl)-1H-pyrazole-3,5-diamine + terephthalaldehyde
PAZm/Py/ZnO_b	5	4-((3-chlorophenyl) diazenyl)-1H-pyrazole-3,5-diamine + terephthalaldehyde
PAZm/Py/ZnO_c	5	4-((4-chlorophenyl) diazenyl)-1H-pyrazole-3,5-diamine + terephthalaldehyde

2.4. Fabrication of polymer nanocomposites PAZm/Py/ZnO_{a-c} (5%)

The PAZm/Py/ZnO_{a-c} nanocomposites were fabricated by using the same synthesis technique with the assistance of ultrasonics throughout the following procedures: 1 mole of diaminopyrazole derivatives **5d-f** and 5% loading Zinc oxide nanoparticles (ZnONPs) was dissolved in suitable amount of ethanol using ultrasonicator for 10 min at 60℃. Then 1 mole of terephthalaldehyde was added in the presence few drops of glacial acetic acid. In a three-necked flask equipped with a condenser inside a system saturated with dry nitrogen, inlet and outlet, the previous reaction mixture was heated under a magnetic stirrer for 8 hours at 70–80 ℃. Then by filtration, the polymer precipitated was isolated and it was washed with hot ethanol then left to dry at room temperature. The polymer nanocomposites are presented in Table 1.

2.4.1. PAZm/Py/ZnO_a nanocomposites

PAZm/Py/ZnO_a nanocomposites was fabricated in the presence of 1 mole (1.18 g) of monomer **e** with 1 mole (0.67 g) of terephthalaldehyde by adding 5% (0.071 g) ZnONPs as the same procedure previously discussed. FT-IR: 1610 cm^{-1} (C=N), 2934 cm^{-1} (=C-H stretching of aliphatic), 3240 cm^{-1} (N-H of pyrazole), 1461 cm^{-1} and 1558 cm^{-1} (C=C of the aromatic), 3063 cm^{-1} (C-H stretching of aromatic), 751 cm^{-1} (C-Cl), 500–800 cm^{-1} (Zn-O).

2.4.2. PAZm/Py/ZnO_b nanocomposites

PAZm/Py/ZnO_b nanocomposites was fabricated in the presence of 1 mole (0.59 g) of monomer **f** with 1 mole (0.33 g) of terephthalaldehyde by adding 5% (0.058 g) ZnONPs as the same procedure previously discussed. FT-IR: 1607 cm^{-1} (C=N), 2889 cm^{-1} (=C-H stretching of aliphatic), 3284 cm^{-1} (N-H of pyrazole), 1467 cm^{-1} and 1605 cm^{-1} (C=C of the aromatic), 3051 cm^{-1} (C-H stretching of aromatic), 783 cm^{-1} (C-Cl), 500–800 cm^{-1} (Zn-O).

2.4.3. PAZm/Py/ZnO_c nanocomposites

PAZm/Py/ZnO_c nanocomposites was fabricated in the presence of 1 mole (0.78 g) of monomer **c** with 1 mole (0.44 g) of terephthalaldehyde by adding 5% (0.046 g) ZnONPs as the same procedure previously discussed. FT-IR: 1627 cm^{-1} (C=N), 2884 cm^{-1} (=C-H stretching of aliphatic), 3261 cm^{-1} (N-H of pyrazole), 1477 cm^{-1} and 1602 cm^{-1} (C=C of the aromatic), 3050 cm^{-1} (C-H stretching of aromatic), 800 cm^{-1} (C-Cl), 500–800 cm^{-1} (Zn-O).

2.5. Characterization techniques

2.5.1. Viscosity measurements

The inherent viscosities of these new polyazomethine polymers were determined in DMSO at 35°C with an Ubbelohde suspended-level viscometer. The value is defined as:

$$\eta inh = 2.3 \log(\eta rel.)/C$$

Where C represents the mass concentration of the polymer (g/dL) and η_{rel} is the relative viscosity, which is defined as $\eta_{rel} = \eta/\eta_o$ where η is the viscosity of the solution and η_o is the viscosity of the solvent. Solution concentrations were 0.5 g/100 mL and the viscosity ratio is η/η_o.

2.5.2. Solubility

The solubility of these new polyazomethine polymers was evaluated under the same conditions with various solvents. 5 mg of each polymer was dissolved in 1 mL of the desired solvent. The solvents that were used included: dimethyl sulfoxide (DMSO), acetone, formic acid, concentrated H_2SO_4, dichloromethane (DCM), tetrahydrofuran (THF), and dimethylformamide (DMF).

2.5.3. Thermal analyses

Thermogravimetric analysis (TGA), and differential thermogravimetric (DTG), were carried out using a Shimadzu TG-50 H thermal analyzer at temperatures rising from air temp to 800 °C and a heating rate of 10 °C/min under a nitrogen atmosphere

2.5.4. Molecular weight determination

Gel permeation chromatography (GPC) was the original technique used to determine the molecular weight. GPC measurements of the new polyazomethine polymers were possessed through Agilent-GPC Agilent Technologies in Germany. G-1362A was the refractive index detector with 100-104-105 A° Altra-styragel columns connected in series. The eluent was THF at a flow rate of 1 mL min^{-1} and in the presence of reference

polymer (PS polystyrene). The GPC equipment was run under the following situations: flow rate = 2.000 mL min^{-1}, injection volume = 100.000 µL, and sample concentration = 1.000 g L^{-1}.

2.5.5. X-Ray diffraction (XRD)

The XRD of polymers and their nanocomposites was recorded using (XRD) D8 ADVANCE in the range 2θ between 5° and 80° at 40 kV voltage and 40 mA using Cu-Kα radiation.

2.6. Antimicrobial activity

2.6.1. Antimicrobial screening for PAZm/$Py_{4–6}$ polymers

From 48-hour-old cultures grown on nutrient agar in sterile water, a cell suspension of each bacterial strain was made [62,63]. One milliliter of the cell suspension was added to a Petri dish (9 cm in diameter); then 15 mL of NA was poured onto the plate. The inoculum was homogenized by a light shake of the plate. An Ampicillin solution was used as a reference drug and was impregnated with solutions of the tested PAZm/$Py_{4–6}$ polymers (0.1 and 0.05 mg/mL in DMSO) on sterile 5-mm filter paper discs (Whatman). As a control, additional discs were impregnated with the solvent (DMSO). After drying for 1 hour, the impregnated discs were placed in the middle of each plate. The seeded plates were incubated for 24–48 hours at 25 ± 3 °C. The triplicate sets' inhibition zone radii (in millimeters) were measured; the results are shown in Table 6.

From a culture of the test fungi growing on potato dextrose agar or sabouraud agar media (SDA) that was 2 to 5 days old, a spore suspension in sterile water was prepared [62,63]. The final spore concentration was 5×10^5 spores/mL. A sterile Petri dish measuring 9 cm in diameter was filled with approximately 15 mL of the growth medium, and 1 mL of the spore suspension was added for inoculation. The inoculum was homogenized by a light shake of the plate. Using the conventional agar disc diffusion method, the antifungal activity of the PAZm/$Py_{4–6}$ polymers was evaluated as follows: Dermatin was used as a reference drug and was impregnated with solutions of the test polymers (0.1 or 0.05 mg/mL in DMSO) on sterile 5-mm filter paper discs (Whatman). Additionally, other discs that served as controls were impregnated with the solvent (DMSO). After drying for 1 hour, the impregnated discs were placed in the middle of each plate. The seeded plates were incubated at 25 ± 3 °C for 5 days. Throughout the incubation period, successive measurements of the inhibition zone radii (in millimeters) were taken. Triplicate sets were applied for each treatment, and the results are shown in Table 6.

2.6.2. Antimicrobial activity for PAZm/Py/ZnO_{a-c} nanocomposites

The antimicrobial activities of the newly fabricated nanocomposites were evaluated using the agar diffusion method with various bacterial and fungal species, including the *Staphylococcus aureus* (ATCC 29,213) and *Bacillus Cereus* (ATCC 14,579) as selected Gram-positive bacteria strains, *Escherichia coli* (ATCC 35,218) and *Serratia marcescens* (ATCC 21,074) as selected Gram-negative bacteria strains, and *Aspergillus flavus* (ATCC 9643) and *Candida albicans* (ATCC 76,615) as selected fungi. All organisms were obtained from microbiology lab, National Research Center, Cairo. Previous literature has described the method used to evaluate the new nanocomposites' antimicrobial effectiveness [64]. Briefly, a 90 mm Petri dish was filled with 25 mL of Muller-Hinton agar; 200 µL of bacterial cultures were autoclaved for 25 min and then spread on the surface of the agar plates using sterile swabs. The targeted materials were cut into 6 mm diameter disk specimens. The discs were washed with distilled water and disinfected at 120°C/20 min. The discs were then placed on the surface of the media. Finally, the Petri dishes were incubated at 30 °C for 24–48 h. The results of measuring the growth inhibition zone's size are shown in Table 6.

3. Results and discussion

3.1. Syntheses of monomers and PAZm/$Py_{4–6}$ polymers

The syntheses of monomers are shown in Figure 1. Sodium nitrite solution was added to the solutions of aniline hydrochloride derivatives to form the diazonium salts of aniline derivatives. The appropriate arylamines are diazotized, then condensed with malononitrile, yielded the precursor hydrazones 4. The latter derivatives were cyclized with hydrazine hydrate to obtain diaminopyrazole derivatives 5 [59–61]. The melting points for the synthesized monomers have been measured and the result was in agreement with literature [59].

Moreover, and as shown in Figure 2, by using the polycondensation reaction under a nitrogen atmosphere, the interaction between terephthalaldehyde and diaminopyrazole derivatives (d-f) in absolute ethanol and the presence of a few drops of glacial acetic acid resulted in the formation of a novel series of polyazomethine containing a pyrazole moiety in the polymer backbone.

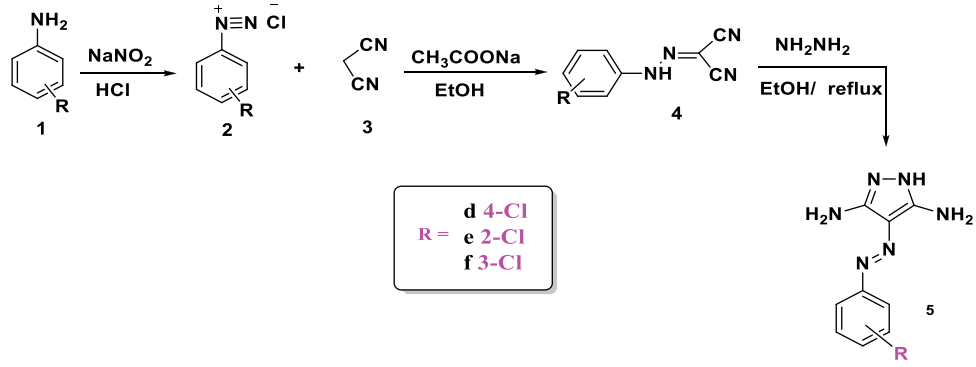

Figure 1. Synthesis of monomers.

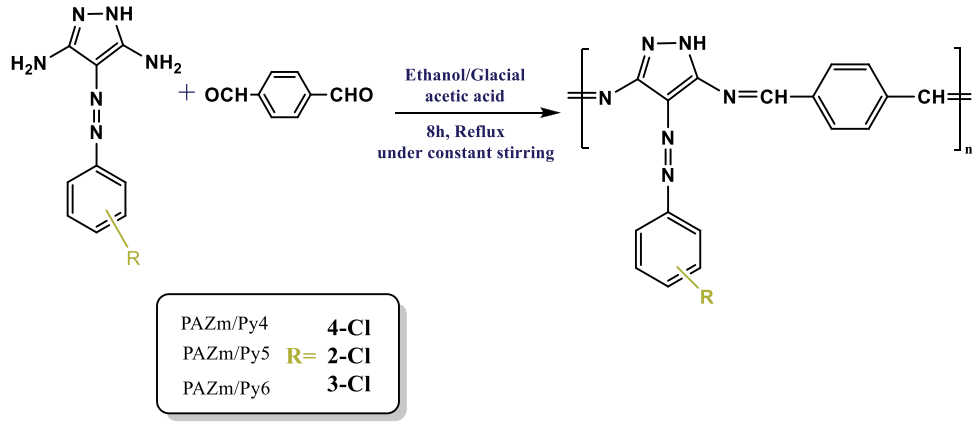

Figure 2. Synthesis of PAZm/$Py_{4–6}$.

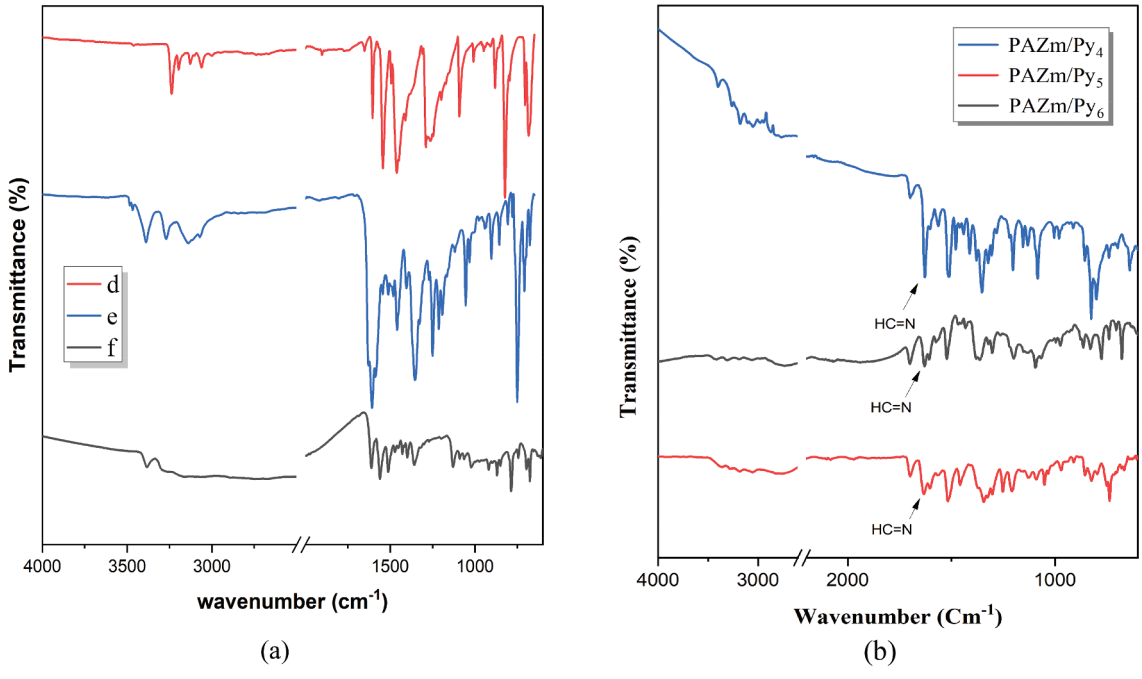

Figure 3. FT-IR spectra for (a) monomers (5d-f) and (b) PAZm/$Py_{4–6}$.

FT-IR analysis was used to characterize the monomers, and the results are discussed in the experimental section, which confirmed the expected structures as displayed in Figure 3(a).

The chemical structure of these new polymers was examined by FT-IR and ^{1}HNMR analysis is presented in the experimental section. The characterization of the resultant PAZm/Py$_{4-6}$ structure was done by using FT-IR analysis and is presented in Figure 3(b). The peak of absorption visible at 1627–1634 cm^{-1} indicates azomethine (HC=N) stretching vibrations, that confirmed the formation of the azomethine linkage [65]. As a result of the change in the location of C – Cl in the aromatic structure, a C – Cl peak was observed in PAZm/Py$_{\mathbf{5}}$ at 737 cm^{-1}, while in PAZm/Py$_{\mathbf{6}}$ it was observed at 773 cm^{-1} and in PAZm/Py$_{\mathbf{4}}$ at 802 cm^{-1}. The perception found in the FT-IR spectra indicates that PAZm/Py$_{4-6}$ was synthesized successfully.

Different standard characterization tools, such as solubility tests, GPC molecular weight determinations, XRD analysis, thermal properties, and SEM, were used to characterize the new polyazomethine derivatives as following:

The solubility of these new polyazomethine polymers was evaluated under the same conditions with various solvents. 5 mg of each polymer was dissolved in 1 ml of the desired solvent. The solvents that were used included dimethyl sulfoxide (DMSO), acetone, formic acid, concentrated H_2SO_4, dichloromethane (DCM), tetrahydrofuran (THF), and dimethylformamide (DMF). The inherent viscosities of these new polyazomethines were determined by using an Ubbelohde suspended-level viscometer in DMSO at 35°C. Table 2 provides a list of the results. From the data presented, at room temperature, all the PAZm/Py$_{4-6}$ were completely soluble in the following solvents: concentrated H_2SO_4, Formic acid, DMF, DMSO, and THF, while they were completely insoluble in both Acetone and DCM.

The average molecular weights of the synthesized polyazomethines are displayed in Table 3 PAZm/Py$_6$ showed a molecular weight with a weight-average of 26,278.16, which was a result of repeating Pw ~ 79 units. While PAZm/Py$_5$ gave an Mw of 25,628.48, Pw= ~ 77, and PAZm/Py$_4$ gave an Mw of 28,939.07, Pw= ~ 87, the PDI of PAZm/Py 4,5, and 6 was 1.13, 1.12, and 1.19, respectively. Furthermore, the inherent viscosities of these new polyazomethine polymers were determined by using an Ubbelohde suspended-level viscometer in DMSO at 35°C. As shown in Table 3, the viscosity of PAZm/Py$_4$ was the highest (1.23 dL/g). This could be due to the polymer's high molecular weight. The $\boldsymbol{\eta_{inh}}$ of PAZm/Py$_6$ and PAZm/Py$_5$ was 1.19 dL/g and 1.08 dL/g, respectively. All polymers had nearly similar $\boldsymbol{\eta_{inh}}$ values since their average molecular weights were likely similar. The results of the viscosity measurements were matched with the GPC data.

PAZm/Py$_{4-6}$ were studied at room temperature using XRD to obtain information about their crystallinity over the 2θ range of 5°–80°. The nature of PAZm/Py$_{4-6}$ was shown in Figure 4. The measurements give several sharp peaks with different intensities at 2θ = 9.9°, 10.8°, 13.9°, 14.6°, 17.5°, 18.5°, 20.4°, 21.2°, 22.6°, 23.3°, 25.1°, and 27.9° for all polymers. The investigated polymers showed normal crystalline structures.

The thermal behavior of PAZm/Py$_{4-6}$ was carried out by TGA at temperatures ranging from air temperature to 800°C under a nitrogen atmosphere. As outlined in Figure 5(a), PAZm/Py$_{4-6}$ thermographs showed the same decomposition pattern. Thermal data showed that the polymers were remarkably thermally stable up

Table 2. Solubility characteristics of PAZm/Py$_{4-6}$.

Materials	DMF	DMSO	THF	Acetone	DCM	Sulfuric acid	Formic acid	η_{inh} (dL/g)
PAZm/Py$_4$	++	++	++	–	–	++	++	1.23
PAZm/Py$_5$	++	++	++	–	–	++	++	1.08
PAZm/Py$_6$	++	++	++	–	–	++	++	1.19

++ Soluble at room temperature.
+ Partially soluble.
– Insoluble.

Table 3. The GPC results for PAZm/Py$_{4-6}$.

		GPC results			
Materials	M. formula	[a]Mw	[b]Mn	[c]Pw	PDI
PAZm-Py$_5$	$(C_{17}H_{11}ClN_6)_n$	25628.48	22793.81	~ 77	1.12
PAZm-Py$_6$	$(C_{17}H_{11}ClN_6)_n$	26278.16	21998.73	~ 79	1.19
PAZm-Py$_4$	$(C_{17}H_{11}ClN_6)_n$	28939.07	25538.93	~ 87	1.13

[a]Weight-average molecular weight.
[b]Number-average molecular weight.
[c]Average number of repeating units.

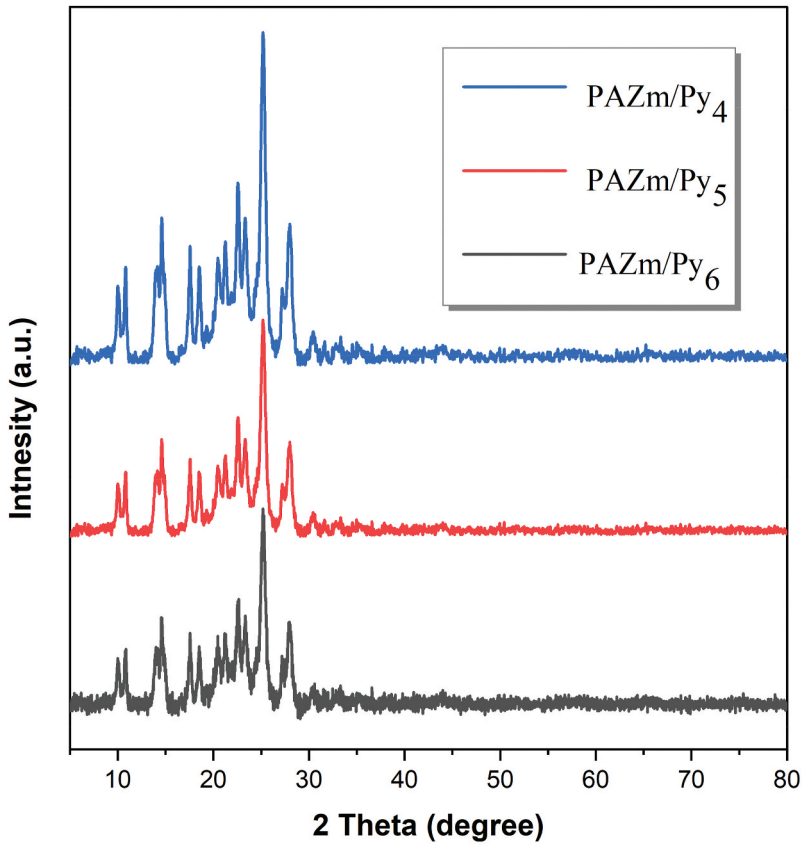

Figure 4. X-ray diffraction charts of the polymers.

to 800 °C. Polymer decomposition was a three-step process. The first step was between 31°C and 249°C. There was an overlap between the second and third steps of degradation between ~ 290 and 630°C. The rate of degradation is slightly faster than in the first. The IDT was the temperature at which decomposition could initiate. The initial decomposition temperatures of all of the prepared PAZM/$Py_{4–6}$ appeared to be 10% weight loss percentage temperatures (T_{10}). They were in the range of 276–331°C.

As a result, the information in Table 4 indicates that the thermal stabilities of PAZm/$Py_{4–6}$ (at 10%) were in the order: PAZm/Py_4 > PAZm/Py_5 > PAZm/Py_6. The T_{50} value is one of the most important criteria for determining a polymer's relative thermal stability. The T_{50} values of the PAZm/$Py_{4–6}$ were discovered after the examination of the data. They were in the 519–583 °C range. The weight loss of the PAZm/Py (4, 5, and 6) at 800 °C was 67%, 95%, and 86%, respectively, which indicates the thermal stability of these polymers.

Moreover, the PDT_{max} values which represent the maximum degradation temperature that may occur for each polymer. PDT_{max} values were determined from the corresponding DTG curves as illustrated in Figure 5(b) and the estimated valued were listed as shown in Table 4. PAZm/Py_4 polymer shows the higher PDT_{max} value while PAZm/Py_5 polymer shows the lowest value

Surface morphologies of the synthesized PAZm/Py_5 and PAZm/Py_6 are displayed in Figure 6 and interpreted by SEM analysis at different magnitudes. According to SEM photographs of PAZm/Py_6 in Figure 6(a,b), it can be observed that aggregated particles (sponge like structure) with a few small round species at magnifications of (a, b X = 12000, c X = 24000). The SEM image of PAZm/Py_5 can be seen in Figure 6(c-e). We can observe a merged globular particle in the range of 631,4 nm to 987.2 nm at a magnification of X = (15000, 30000, 60000) c, d, and e, respectively.

3.2. *Fabrication PAZm/Py/ZnO_{a-c} nanocomposites*

A new set of composite materials containing polyazomethine and 5% of zinc oxide nanoparticles in the form of PAZm/Py/ZnO_{a-c} were successfully synthesized through the polycondensation polymerization method. The polymerization reactions are the same as the polymerization procedures for pure polyazomethine. The fabrication process is based chiefly on diaminopyrazole derivatives (5a-c) and terephthalaldehyde in the presence of a 5% loading of ZnO NPs. The synthetic route for synthesizing the PAZm/Py/ZnO_{a-c} nanocomposites is

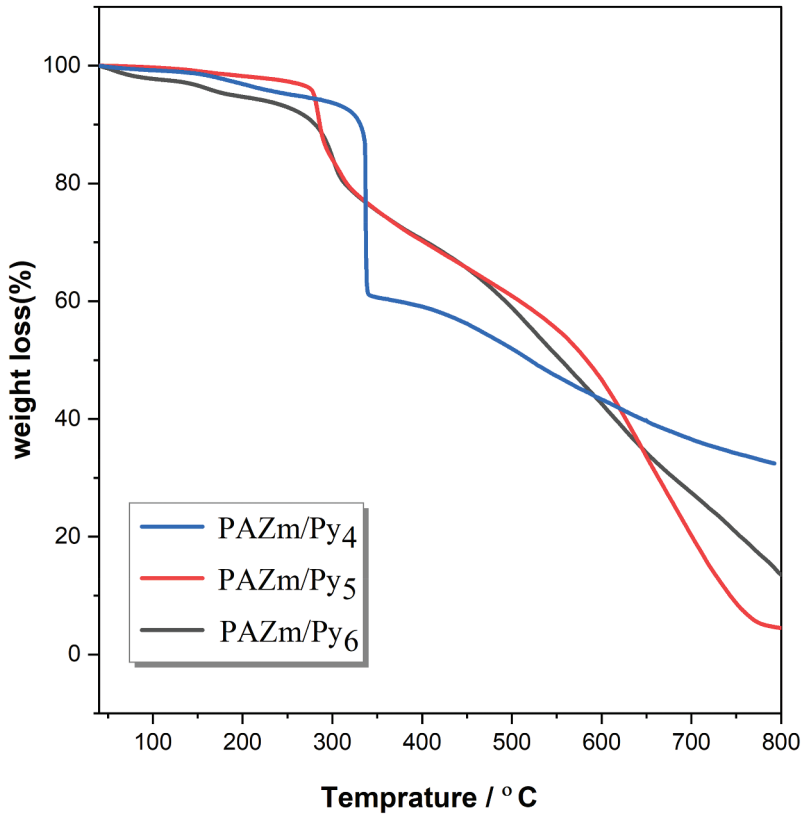

Figure 5a. TGA curves of PAZm/$Py_{4–6}$.

Table 4. Thermal properties of PAZm/$Py_{4–6}$.

		Temperature (°C) for different percentage decompositions [b]				
Polymers	PDT_{max} [a] (°C)	10 %	20 %	30 %	40 %	50 %
PAZm/Py_4	350.29	331	336	337	372	519
PAZm/Py_5	277.72	285	315	402	508	583
PAZm/Py_6	300.81	276	313	404	492	554

[a]The values were determined from DTG curves.
[b]The values were determined by TGA at 10°C per min heating rate.

demonstrated in Figure 7. The chemical structure of these new polymer nanocomposites was gained using FT-IR spectroscopy as explained in the experimental section and presented in Figure 8(a). The absorption bands of PAZm/Py/ZnO_{a-c} nanocomposites are clearly observed to be the same as those of pure PAZm/Py, but the spectrum of pure polyazomethine changes slightly after the immersion of ZnO NPs into the PAZm/Py polymer matrix. The peak of absorption visible at 1604–1626 cm^{-1} indicates to the azomethine (HC=N) stretching vibrations. The absence of (NH_2) and (C=O) peaks suggests the predicted azomethine compound. The presence of metal-oxygen (Zn-O) causes short peaks between 500–800 cm^{-1} [66,67].

The XRD pattern was recorded using (XRD) D8 ADVANCE in the range of 2θ between 5° and 80° and at room temperature. The XRD patterns of PAZm/Py/ZnO_{a-c} nanocomposites are shown in Figure 8(b), which confirms the synthesis of PAZm/Py/ZnO_{a-c} nanocomposites. As mentioned earlier, the pure polymer has a crystalline nature where it shows all peaks correspond to the pure polymer. Moreover, the XRD pattern of PAZm/Py/ZnO_{a-c} shows diffraction peaks at 2θ = 31.74° (100), 34.46° (002), 36.28° (101), 47.81° (102), 56.70° (110), 62.92° (103), 67.88° (112), and 69.14 (202) corresponding to zinc oxide nanoparticles as mentioned in a previous study [68]. This indicates a good merging of ZnONPs into the matrix of polymers.

The thermal properties of PAZm/Py/ZnO_{a-c} were examined using TGA and DTG under a nitrogen atmosphere at a heating rate of 10 °C per minute. All thermogravimetric (TG) curves are shown in Figure 9(a), and they all show the same pattern of decomposition and a small weight loss that nearly stops before 125 °C. This behavior is caused by the removal of moisture and attached solvents.

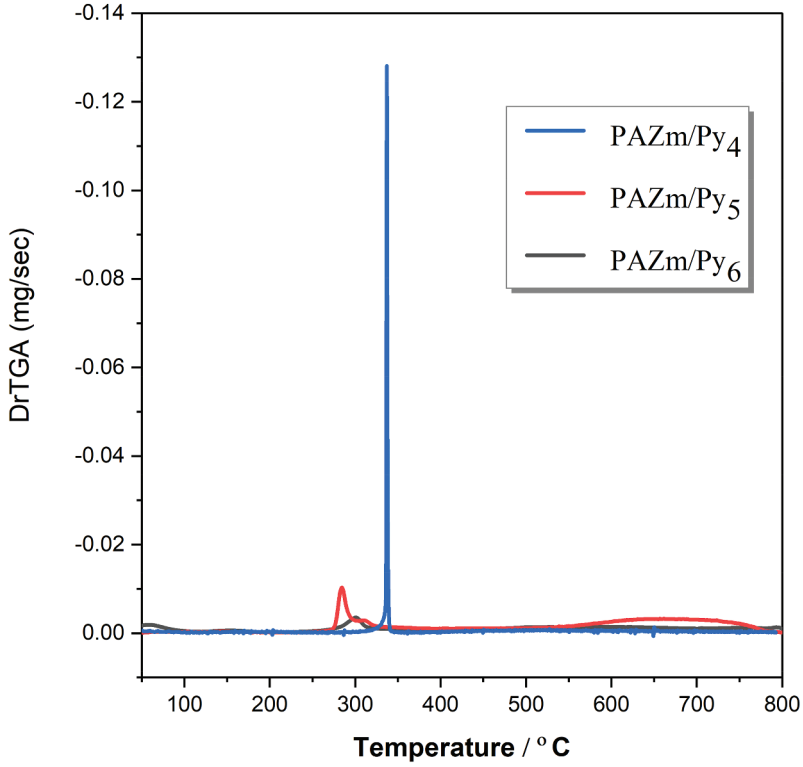

Figure 5b. DTG curves of PAZm/$Py_{4–6}$.

As shown in Table 5, the T_{10}-T_{50} values represent the temperatures for variable percent weight losses of 10%, 20%, 30%, 40%, and 50%. The degradation of polymer nanocomposites occurs mainly in a three-step process. The first step was between 125°C and 241°C. There was an overlap between the second and third steps of degradation. A closer examination of the TG curves reveals that the fast degradation step in all samples begins in all samples at temperatures above 300 °C. This confirms that these materials are thermally stable up to high temperatures. These products begin to decompose a few degrees before T_{10} occurs. As a result, the information in Table 5 indicates that the thermal stabilities of PAZm/Py/ZnO_{a-c} (at 10% weigh losses) were in the order: PAZm/Py/ZnO_b = PAZm/Py/ZnO_c > PAZm/Py/ZnO_a. After analyzing the data, the T_{50} values of the PAZm/Py/ZnO_{a-c} were discovered to be in the range of 491–641 °C. The fabricated PAZm/Py/ZnO (a, b, and c) lost weight at 800 °C at a rate of 74%, 68%, and 75%, respectively. Compared to the pure polymer, the residue of the sample increased for both a and b, and this indicates a thermal improvement after adding the filler.

On the other hand, the composite maximum decomposition temperature is illustrated as CDT_{max} which is referring to the temperature at which the decomposition reaches to the maximum stage. These values are listed in Table 5 and were examined from the corresponding DTG curves for the designed composite materials (Figure 9(b)). The CDT_{max} values display a significant change to lower level compared to the investigated valued for the pure polymers. This is mainly attributed to the presence of ZnO reinforced nanoparticles

The morphological properties of PAZm/Py/ZnO nanocomposites were measured by SEM, EDX, and TEM images. The surface morphologies of the synthesized PAZm/Py/ZnO_a nanocomposites and PAZm/Py/ZnO_b nanocomposites were interpreted by SEM analysis at different magnitudes as displayed in Figure 10. According to SEM photographs of PAZm/Py/ZnO_a in Figure 10(a,b), in addition to the aggregated particles of the pure polymer (sponge-like structure) and a few small round species, the nanoparticles were spherical to sub-spherical in shape, as shown in the SEM image with an excellent and uneven distribution of ZnO NPs at magnifications of (a, X = 50,000; b, X = 100,000). The SEM image of PAZm/Py/ZnO_b can be seen in Figure 10(c,d) at a magnification of X = 50,000 and 100,000, respectively. Polyazomethine and ZnO nanoparticles show merged globular and sub-spherical shapes with an agglomeration of ZnO nanoparticles in some restricted areas on the surface of polyazomethine. The EDX investigation of the synthesized

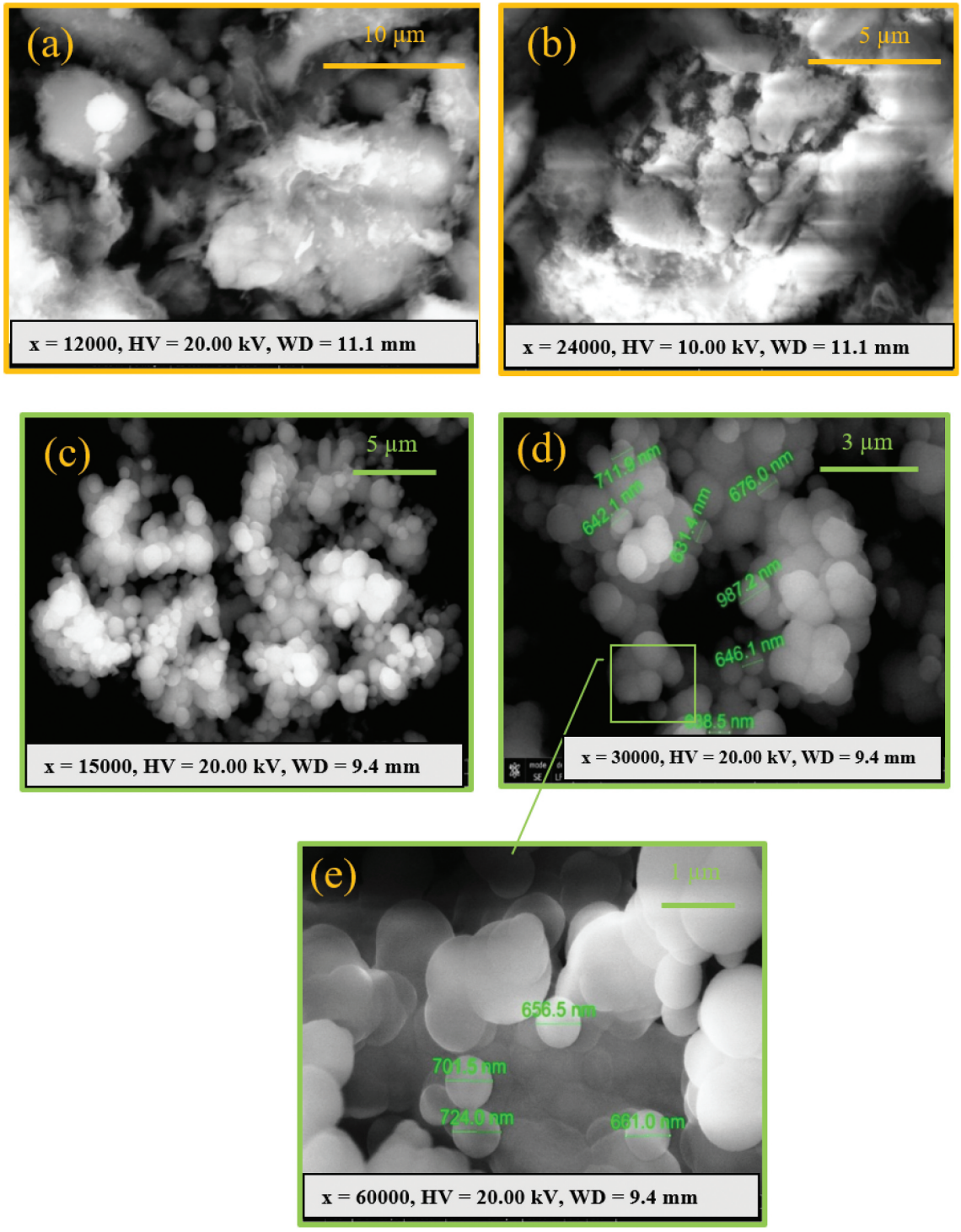

Figure 6. SEM images of PAZm/Py_6 magnifications (a, X=12000 b, X= 24000), PAZm/Py_5 magnification (c, X=15000 d, X=30,000 e, X=60,000).

PAZm/Py/ZnO_b showed the occurrence of carbon, oxygen, and zinc.Figure 11(a) shows the EDX diagram of elements, representing a signal from C (carbon), O (oxygen) and Zn (zinc). Similar peaks were reported in previous studies [67,68], which clearly confirms the presence of ZnO NPs in the polymer. Figure 11(b-d) shows the distribution combinability of C, O, and Zn in the sample.

The TEM images of PAZm/Py/ZnO_a are displayed in Figure 12(a,b). This figure shows the spherical ZnO nanoparticles dispersed around polyazomethine. While the TEM images of PAZm/Py/ZnO_b are displayed in

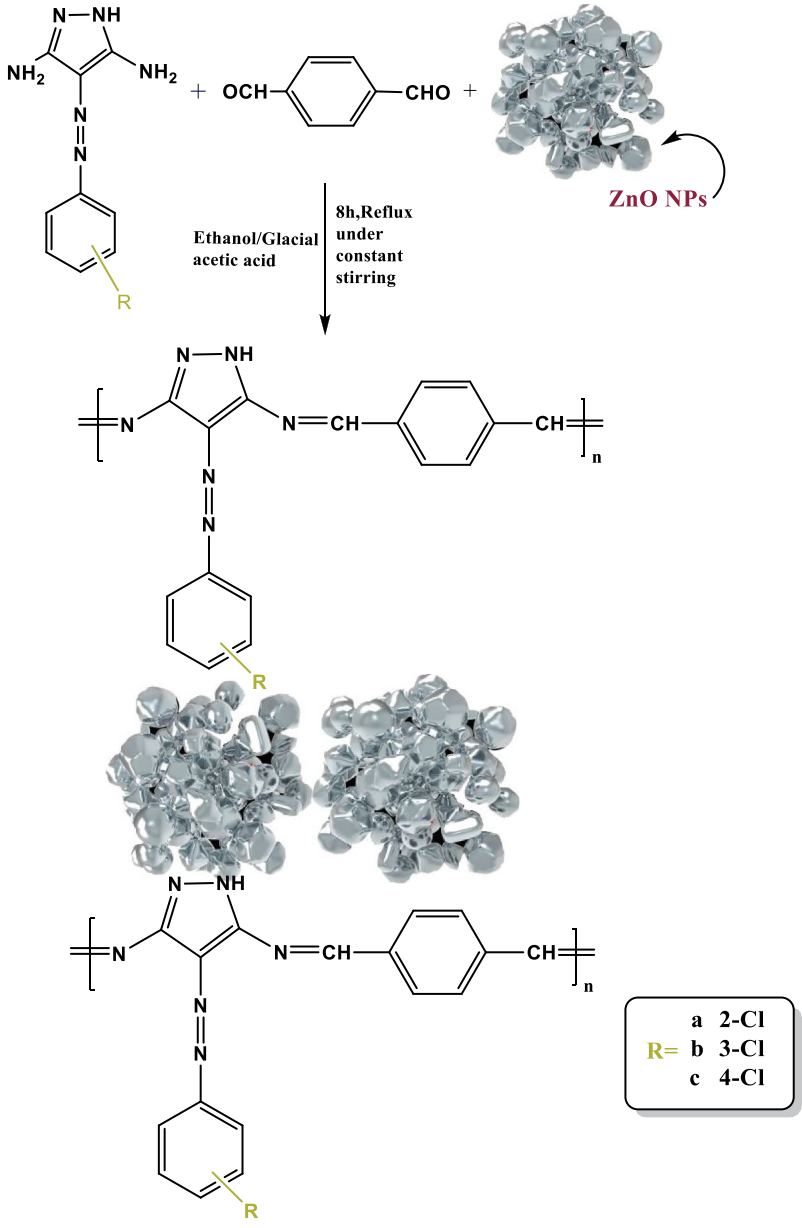

Figure 7. Fabrication of PAZm/Py/ZnO_{a-c}.

Figure 12(c,d), the spherical ZnO nanoparticles dispersed in polyazomethine are shown in this figure with no agglomeration or concentration in any particular area.

3.3. Antimicrobial activity of PAZm/$Py_{4–6}$ and PAZm/Py/ZnO_{a-c}

The antimicrobial activity of all the synthesized PAZm/$Py_{4–6}$ and PAZm/Py/ZnO_{a-c} nanocomposites was done as described in the experimental section [62–64]. The antimicrobial activity of polymers and polymer nanocomposites was tested against some selected bacteria and fungi, including *Staphylococcus aureus* and *Bacillus subtilis* as selected Gram-positive bacteria, *Escherichia coli* and *Serratia marcescens* as selected Gram-negative bacteria, and *Aspergillus flavus* and *Candida albicans* as selected fungi. The inhibition area was introduced in mm and all antimicrobial results have been listed in Table 6.

The results revealed that all tested compounds were found to be effective against the gram-negative bacteria *E. coli* with a zone of inhibition ranging between 2 mm and 14 mm, while the effect against *S. marcescens* was ranging between 3 mm and 13 mm. On the basis of the maximum inhibitory effect, the synthesized polymer PAZm/Py/ZnO_c shows the highest activity against the two types of gram-negative bacteria. On the other hand, most tested

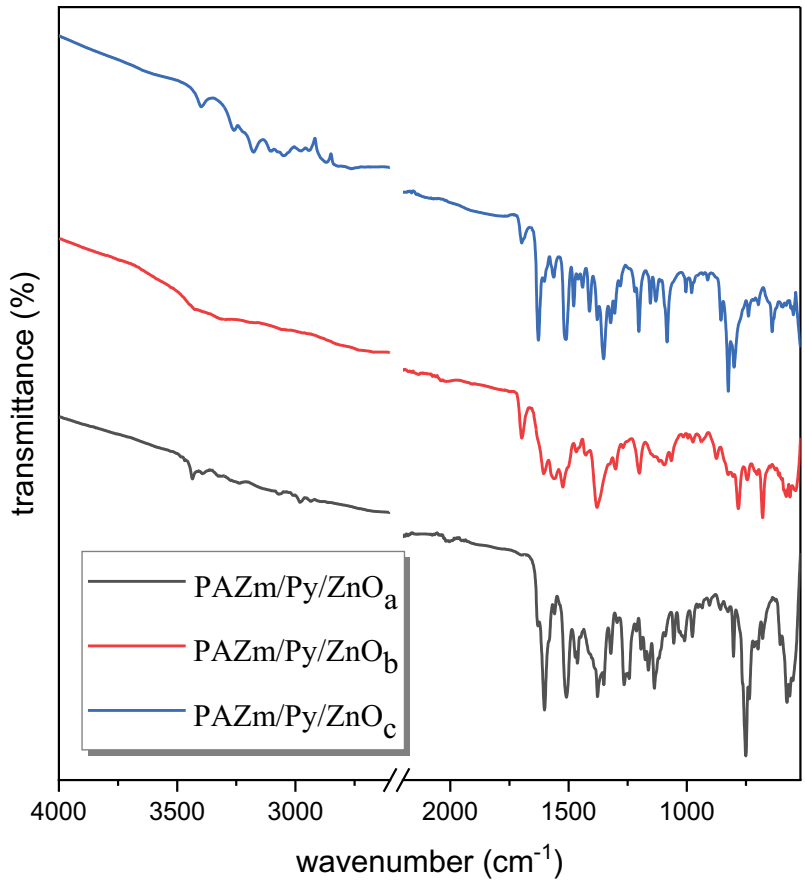

Figure 8a. FT-IR spectra of PAZm/Py/ZnO$_{a-c}$.

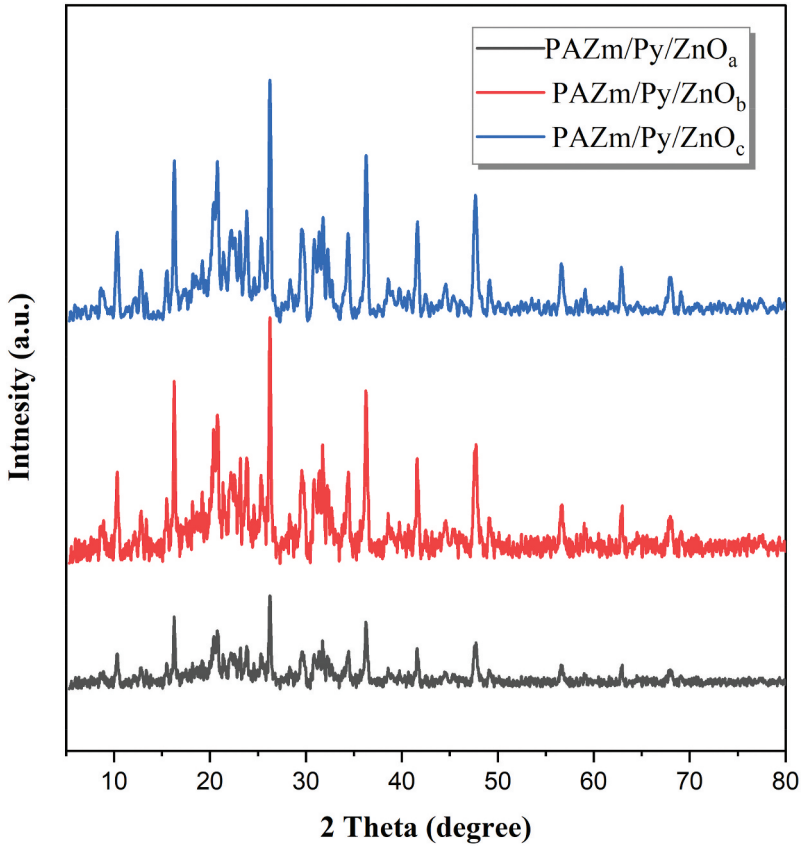

Figure 8b. X-ray diffraction charts of PAZm/Py/ZnO$_{a-c}$.

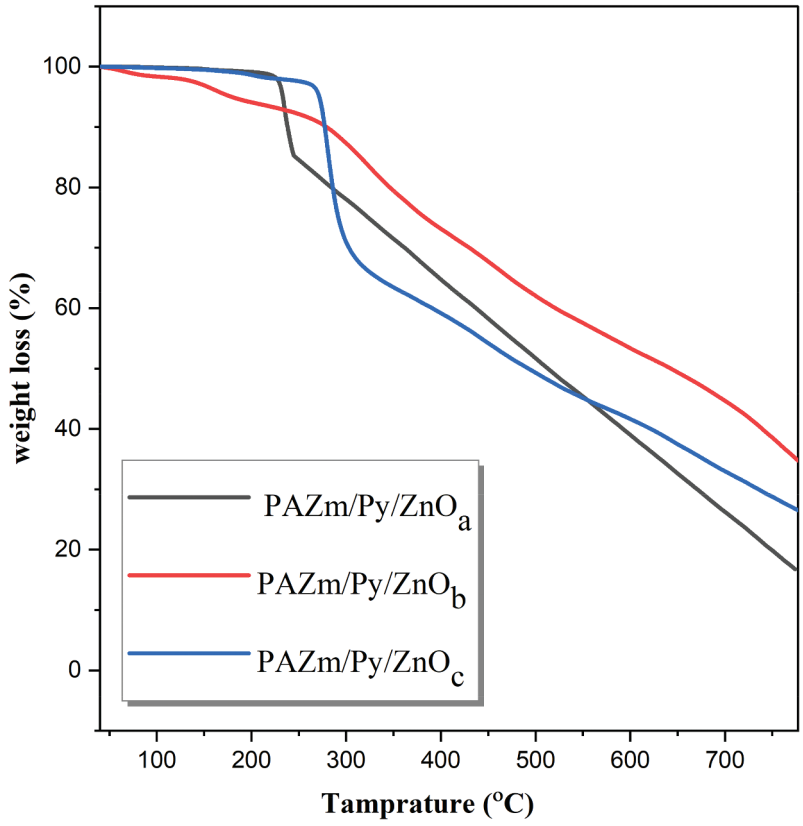

Figure 9a. TGA curves of PAZm/Py/ZnO_{a-c}.

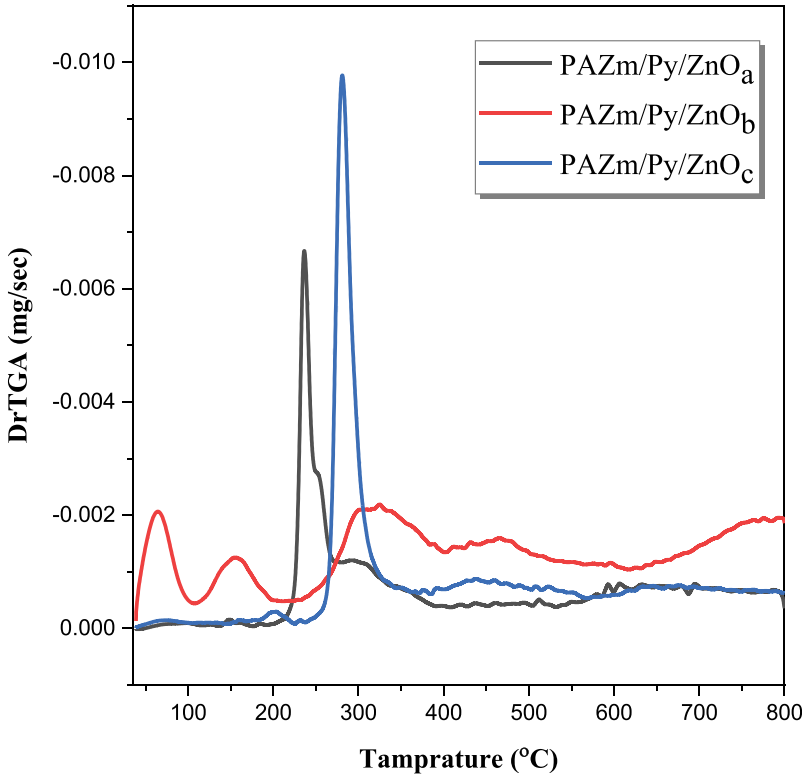

Figure 9b. DTG curves of PAZm/Py/ZnO_{a-c}.

Table 5. Thermal properties of PAZm/Py/$ZnO_{a-c.}$

		Temperature (°C) for different percentage decompositions[b]					
Materials	CDT_{max}[a] (°C)	T_{10}	T_{20}	T_{30}	T_{40}	T_{50}	%Residual
PAZm/Py/ZnO_a	236	238	256	386	462	539	26%
PAZm/Py/ZnO_b	309	277	345	430	520	641	32%
PAZm/Py/ZnO_c	280	277	285	302	390	491	25%

[a]The values were determined from DTG curves.
[b]The values were determined by TGA at 10°C per min heating rate.

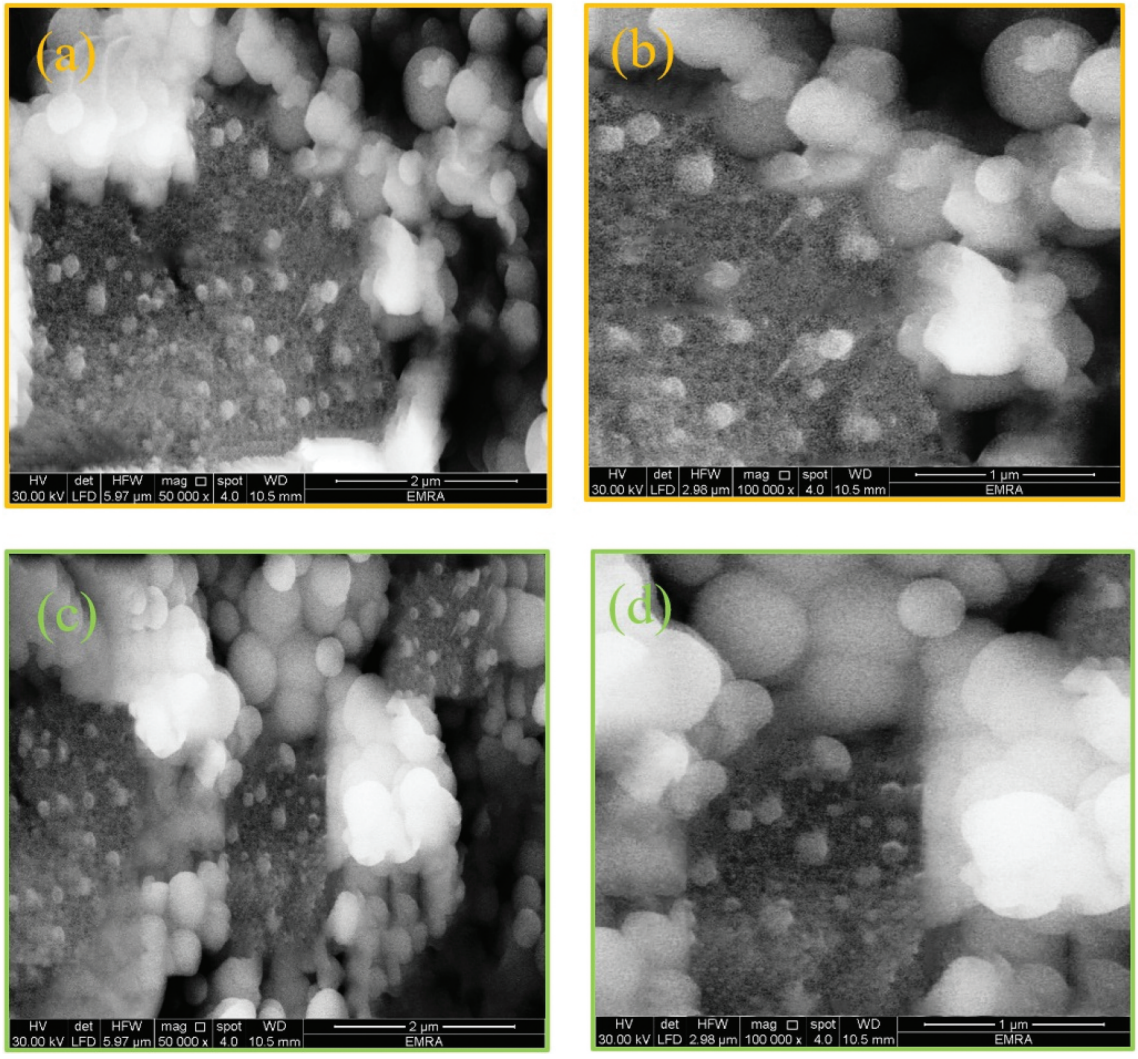

Figure 10. SEM micrographs for PAZm/Py/ZnO_a (a,b) magnifications (x=50,000, 100,000), PAZm/Py/ZnO_b (c,d) magnification (X= 50000 and 100,000).

compounds were found to be variable effective against the gram-positive bacteria except PAZm/Py_5 and PAZm/Py_6 which do not exhibit any activity. As for the effectiveness of synthesized PAZm/$Py_{4–6}$ and PAZm/Py/ZnO_{a-c} nanocomposites against the selected fungi, all prepared compounds showed activity against *A. flavus* with a 2 mm to 10 mm zone of inhibition, while they did not show any antifungal activity against *C. albicans* except PAZm/Py_4 and PAZm/Py/ZnO_c, which showed an antifungal effect with a zone of inhibition of 11 mm for both of them. The antimicrobial activity diagrams of PAZm/$Py_{4–6}$ polymers and PAZm/Py/ZnO_{a-c} nanocomposites against the selected Gram-positive, Gram-negative bacteria and fungi have been illustrated in Figure 13.

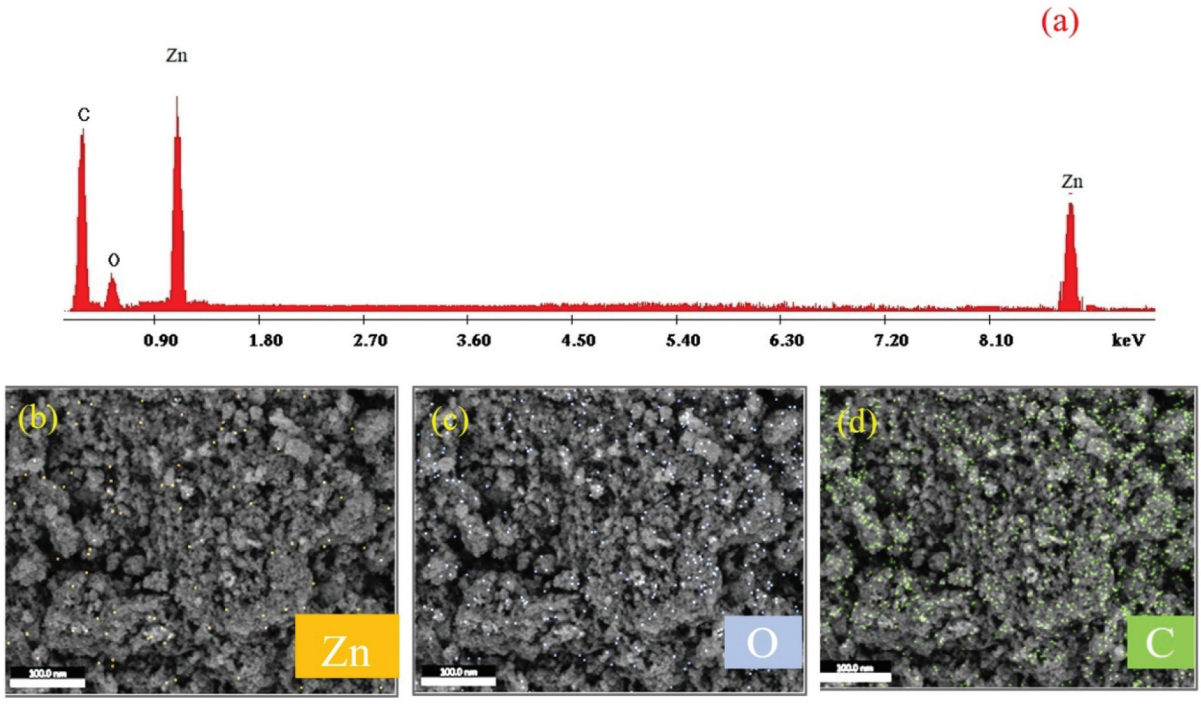

Figure 11. (a) EDX spectrum of PAZmPy/ZnO_b, and (b-d) their corresponding elemental EDX mapping images.

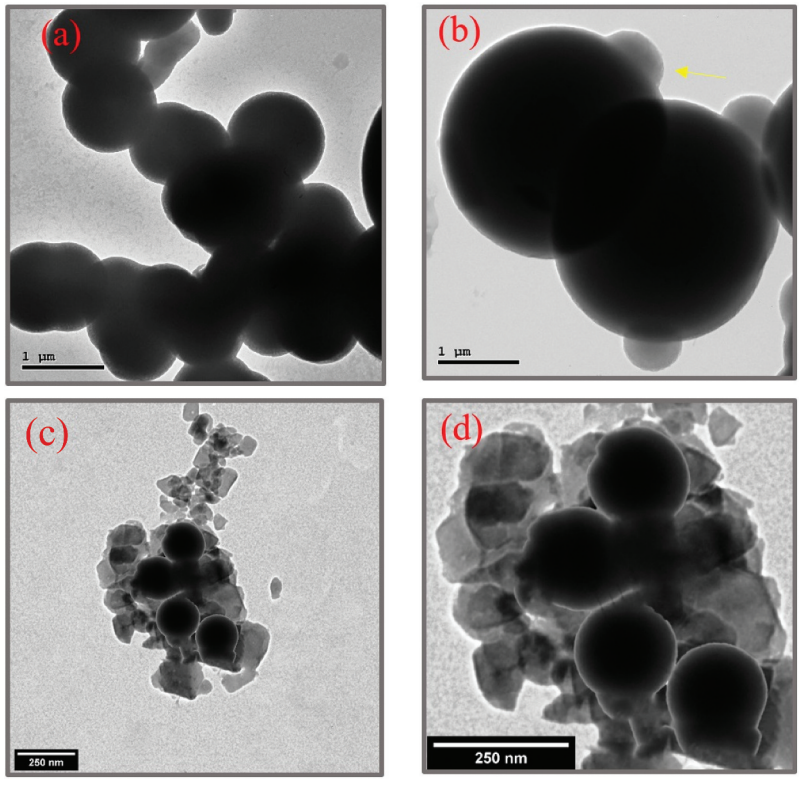

Figure 12. TEM micrographs for PAZmPy/ZnO_a (a,b),PAZm/Py/ZnO_b (c,d).

Table 6. Antimicrobial activity of PAZm/$Py_{4–6}$ polymers and PAZm/Py/ZnO_{a-c} nanocomposites.

	Bacterial species and fungi/Inhibition zone (mm)					
Code	*E. coli*	*S. marcescens*	*B. subtilis*	*S. aureus*	*C. albicans*	*A. flavus*
PAZm/Py_4	12	12	4	6	11	9
PAZm/Py_5	2	3	-	-	-	2
PAZm/Py_6	6	4	-	-	-	3
PAZm/Py/ZnO_a	3	5	1	2	-	2
PAZm/Py/ZnO_b	7	6	1	3	-	4
PAZm/Py/ZnO_c	14	13	6	8	11	10

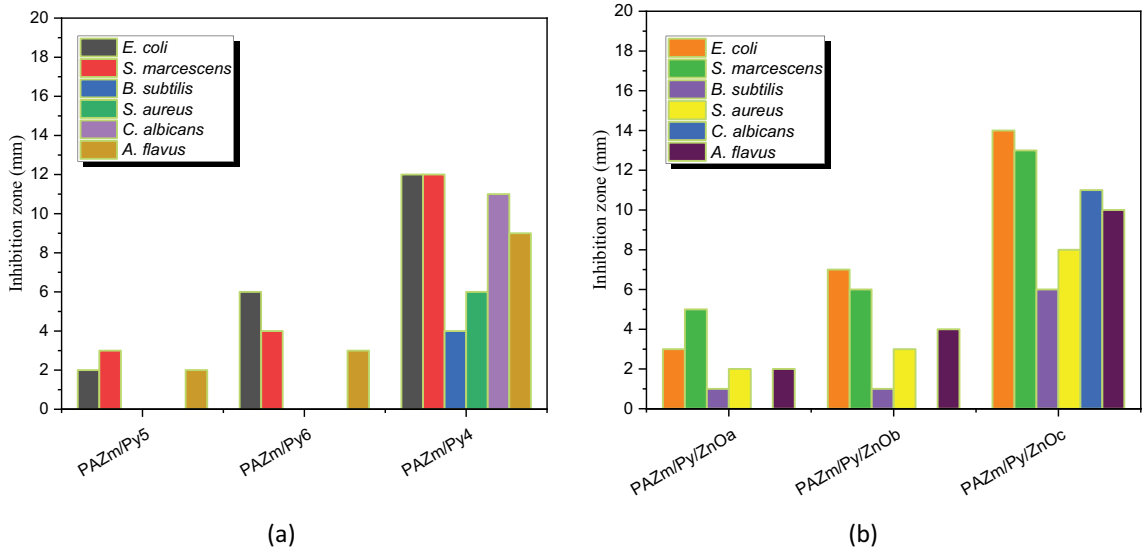

Figure 13. Antimicrobial activity diagram of PAZm/$Py_{4–6}$ polymers (a) and PAZm/Py/ZnO_{a-c} nanocomposites (b) against the selected gram positive, gram negative bacteria and fungi.

4. Conclusion

A new group polyazomethine based on the pyrazole moiety and containing Cl substitution in the different positions (ortho, meta, and para) was synthesized using the polycondensation technique. The polycondensation technique, with the help of ultrasonic assistance, was then used to create polymer nanocomposites of these polymers with a 5% loading of ZnO nanoparticles. The resulting polymers were given the abbreviation PAZm/$Py_{4–6}$, and the polymer nanocomposites of these polymers were made in the form of PAZm/Py/ZnO_{a-c}. The produced polymer and its nanocomposites were identified by IR spectroscopy. GPC analysis and solubility tests were used to investigate the polymers. Additionally, TGA, XRD, and SEM were used to characterize both the polymer and its nanocomposites. The XRD results show that the investigated polymers showed normal crystalline structures and the XRD images of nanocomposites indicates a good merging of ZnONPs into the matrix of polymers. The Incorporating the ZnONPs into polyazomethine matrix relatively improved the thermal stability. The antimicrobial activity of polymers and polymer nanocomposites was tested against some selected bacteria and fungi. The results revealed that all tested compounds were found to be effective against the gram-negative bacteria E. coli and S. marcescens. The synthesized polymer PAZm/Py/ZnO_c shows the highest activity against the two types of gram-negative bacteria. Most tested compounds were found to be effective against gram-positive bacteria except PAZm/Py_5 and PAZm/Py_6, which do not exhibit any activity. As for the effectiveness of synthesized PAZm/$Py_{4–6}$ and PAZm/Py/ZnO_{a-c} nanocomposites against the selected fungi, all prepared compounds showed activity against *A. flavus*, while they did not show any antifungal activity against *C. albicans* except PAZm/Py_4 and PAZm/Py/ZnO_c.

Disclosure statement

No potential conflict of interest was reported by the author(s).

Funding

This research work was funded by Institutional Fund Projects under grant no. (IFPDP-296-22). The authors gratefully acknowledge the technical and financial support provided by

the Ministry of Education and King Abdulaziz University, DSR, Jeddah, Saudi Arabia.

ORCID

Mahmoud A. Hussein http://orcid.org/0000-0002-5128-5136

References

[1] Adams R, Bullock J, Wilson W. Contribution to the structure of benzidine. J Am Chem Soc. 1923;45(2):521–527. doi: 10.1021/ja01655a032

[2] Grigoras M, Catanescu CO. Imine oligomers and polymers. J Macromol Sci Part C Polym Rev. 2004;44 (2):131–173. doi: 10.1081/MC-120034152

[3] Yang CJ, Jenekhe SA. Conjugated aromatic poly (azomethines). 1. Characterization of structure, electronic spectra, and processing of thin films from soluble complexes. Chem Mater. 1991;3(5):878–887. doi: 10.1021/cm00017a025

[4] Jenekhe SA, Yang CJ, Vanherzeele H, et al. Cubic nonlinear optics of polymer thin films. Effects of structure and dispersion on the nonlinear optical properties of aromatic Schiff base polymers. Chem Mater. 1991;3 (6):985–987. doi: 10.1021/cm00018a001

[5] Yang CJ, Jenekhe SA. Effects of structure on refractive index of conjugated polyimines. Chem Mater. 1994;6 (2):196–203. doi: 10.1021/cm00038a016

[6] Yang C-J, Jenekhe SA. Conjugated aromatic polyimines. 2. Synthesis, structure, and properties of new aromatic polyazomethines. Macromolecules. 1995;28 (4):1180–1196. doi: 10.1021/ma00108a054

[7] Kaya İ, Çulhaoğlu S. Syntheses and characterizations of oligo (azomethine ether) s derived from 2, 2′-[1, 4-enylenebis (methyleneoxy)] dibenzaldehyde and 2, 2′-[1, 2-phenylenebis (methyleneoxy)] dibenzaldehyde. Chin J Polym Sci. 2012;30(5):682–693. doi: 10.1007/s10118-012-1143-1

[8] Mirkin MV, Bard AJ. Voltammetric method for the determination of borohydride concentration in alkaline aqueous solutions. Anal Chem. 1991;63(5):532–533. doi: 10.1021/ac00005a030

[9] Ferreira MDL, Vasconcelos TRA, de Carvalho EM, et al. Synthesis and antitubercular activity of novel Schiff bases derived from D-mannitol. Carbohydr Res. 2009;344(15):2042–2047. doi: 10.1016/j.carres.2009.08.006

[10] Zhu H-L, Tong Y-X, Chen X-M. Influence of ligand backbones and counter ions on structures of helical silver (I) complexes with di-Schiff bases derived from phthalaldehydes and diamine. J Chem Soc Dalton Trans. 2000;2000 (22):4182–4186. doi:10.1039/b005228k

[11] Badawi A, Mohamed M, Mohamed MZ, et al. Surface and antitumor activity of some novel metal-based cationic surfactants. J Cancer Res Ther. 2007;3(4):198. doi: 10.4103/0973-1482.38994

[12] Wan-Ren Z, Pei-Zhi H, Mei-Ying L, et al. Synthesis of new Schiff bases containing thiophene moiety. Wuhan Univ J Nat Sci. 2003;8(2):433–436. doi: 10.1007/BF02907226

[13] Negm NA, Zaki MF. Structural and biological behaviors of some nonionic Schiff-base amphiphiles and their Cu (II) and Fe (III) metal complexes. Colloids Surf B Biointerfaces. 2008;64(2):179–183. doi: 10.1016/j.colsurfb.2008.01.018

[14] Barbera J, Oriol L, Serrano J. Hydroxy-functionalized liquid-crystalline polyazomethines I. Synthesis, characterization and structure-mesogenic behaviour relationship. Liq Cryst. 1992;12(1):37–47. doi: 10.1080/02678299208029036

[15] Lee KS, Won JC, Jung JC. Synthesis and characterization of processable conducting polyazomethines. die Makromolekulare Chemie. Macromole Chem Phys. 1989;190(7):1547–1552. doi: 10.1002/macp.1989.021900706

[16] Park SB, Kim H, Zin WC, et al. Synthesis and properties of polyazomethines having flexible (n-alkyloxy) methyl side chains. Macromolecules. 1993;26(7):1627–1632. doi: 10.1021/ma00059a021

[17] Wang C, Shieh S, LeGoff E, et al. Synthesis and characterization of a new conjugated aromatic poly (azomethine) derivative based on the 3 ‘, 4 ‘-dibutyl-α-terthiophene building block. Macromolecules. 1996;29(9):3147–3156. doi: 10.1021/ma9514131

[18] Park KH, Tani T, Kakimoto M-A, et al. Synthesis and characterization of new diphenylfluorene-based aromatic polyazomethines. Macromole Chem Phys. 1998;199(6):1029–1033. doi: 10.1002/(SICI)1521-3935(19980601)199:6<1029:AID-MACP1029>3.0.CO;2-3

[19] Rajendran SP, Sengodan K. Synthesis and characterization of zinc oxide and iron oxide nanoparticles using sesbania grandiflora leaf extract as reducing agent. J Nanoscience. 2017:1–7. doi: 10.1155/2017/8348507

[20] Batool M, Khurshid S, Qureshi Z, et al. Adsorption, antimicrobial and wound healing activities of biosynthesised zinc oxide nanoparticles. Chem Papers. 2021;75 (3):893–907. doi: 10.1007/s11696-020-01343-7

[21] Xing Y, Li W, Wang Q, et al. Antimicrobial nanoparticles incorporated in edible coatings and films for the preservation of fruits and vegetables. Molecules. 2019;24 (9):1695. doi: 10.3390/molecules24091695

[22] Jamdagni P, Khatri P, Rana J. Green synthesis of zinc oxide nanoparticles using flower extract of nyctanthes arbor-tristis and their antifungal activity. J King Saud Univ Sci. 2018;30(2):168–175. doi: 10.1016/j.jksus.2016.10.002

[23] Bekele B, Degefa A, Tesgera F, et al. Green versus chemical precipitation methods of preparing zinc oxide nanoparticles and investigation of antimicrobial properties. J Nanomater. 2021;2021:1–10. doi: 10.1155/2021/9210817

[24] Roy S, Rhim J-W. Carboxymethyl cellulose-based antioxidant and antimicrobial active packaging film incorporated with curcumin and zinc oxide. Int J Biol Macromol. 2020;148:666–676. doi: 10.1016/j.ijbiomac.2020.01.204

[25] Abdelghany TM, Al-Rajhi AMH, Yahya R, et al. Phytofabrication of zinc oxide nanoparticles with advanced characterization and its antioxidant, anticancer, and antimicrobial activity against pathogenic microorganisms. Biomass Convers Biorefin. 2023;13 (1):417–430. doi: 10.1007/s13399-022-03412-1

[26] Chandrasekaran S, Anusuya S, Anbazhagan V. Anticancer, anti-diabetic, antimicrobial activity of zinc oxide nanoparticles: a comparative analysis. J Mol Struct. 2022;1263:133139. doi: 10.1016/j.molstruc.2022.133139
[27] Taghizadeh S-M, Lal N, Ebrahiminezhad A, et al. Green and economic fabrication of zinc oxide (ZnO) nanorods as a broadband UV blocker and antimicrobial agent. Nanomaterials. 2020;10(3):530. doi: 10.3390/nano10030530
[28] Mortezagholi B, Movahed E, Fathi A, et al. Plant-mediated synthesis of silver-doped zinc oxide nanoparticles and evaluation of their antimicrobial activity against bacteria cause tooth decay. Microsc Res Tech. 2022;85(11):3553–3564. doi: 10.1002/jemt.24207
[29] Mahlaule-Glory LM, Hintsho-Mbita NC. Green derived zinc oxide (ZnO) for the degradation of dyes from wastewater and their antimicrobial activity: a review. Catalysts. 2022;12(8):833. doi: 10.3390/catal12080833
[30] Karmous I, Taheur FB, Zuverza-Mena N, et al. Phytosynthesis of zinc oxide nanoparticles using Ceratonia siliqua L. and evidence of antimicrobial activity. Plants. 2022;11(22):3079. doi: 10.3390/plants11223079 Plants.
[31] Thakur S, Shandilya M, Guleria G. Appraisement of antimicrobial zinc oxide nanoparticles through Cannabis Jatropha curcasa Alovera and Tinosporacordifolia leaves by green synthesis process. J Environ Chem Eng. 2021;9(1):104882. doi: 10.1016/j.jece.2020.104882
[32] Maity N, Bruchiel-Spanier N, Sharabani-Yosef O, et al. Zinc oxide nanoparticles embedded photo-crosslinkable PLA-block-PEG toward effective antibacterial coatings. Mater Adv. 2023;4(14):3026–3036. doi: 10.1039/D3MA00169E
[33] Le KH, Nguyen M-B, Tran LD, et al. A novel antimicrobial ZnO nanoparticles-added polysaccharide edible coating for the preservation of postharvest avocado under ambient conditions. Prog Org Coat. 2021;158:106339. doi: 10.1016/j.porgcoat.2021.106339
[34] La DD, Nguyen-Tri P, Le KH, et al. Effects of antibacterial ZnO nanoparticles on the performance of a chitosan/gum Arabic edible coating for post-harvest banana preservation. Prog Org Coat. 2021;151:106057. doi: 10.1016/j.porgcoat.2020.106057
[35] Davies J, Davies D. Origins and evolution of antibiotic resistance. Microbiol Mol Biol Rev. 2010;74(3):417–433. doi: 10.1128/MMBR.00016-10
[36] Krishnamoorthy R, Athinarayanan J, Periasamy VS, et al. Antimicrobial activity of nanoemulsion on drug-resistant bacterial pathogens. Microbial Pathogenesis. 2018;120:85–96. doi: 10.1016/j.micpath.2018.04.035
[37] Lingaraju K, Raja Naika H, Manjunath K, et al. Biogenic synthesis of zinc oxide nanoparticles using ruta graveolens (L.) and their antibacterial and antioxidant activities. Appl Nanosci. 2016;6(5):703–710. doi: 10.1007/s13204-015-0487-6
[38] Sisubalan N, Ramkumar VS, Pugazhendhi A, et al. ROS-mediated cytotoxic activity of ZnO and CeO2 nanoparticles synthesized using the rubia cordifolia L. leaf extract on MG-63 human osteosarcoma cell lines. Environ Sci Pollut Res. 2018;25(11):10482–10492. doi: 10.1007/s11356-017-0003-5
[39] Li Y, Liao C, Tjong SC. Recent advances in zinc oxide nanostructures with antimicrobial activities. Int J Mol Sci. 2020;21(22):8836. doi: 10.3390/ijms21228836
[40] Akbar S, Tauseef I, Subhan F, et al. An overview of the plant-mediated synthesis of zinc oxide nanoparticles and their antimicrobial potential. Inorg Nano-Metal Chem. 2020;50(4):257–271. doi: 10.1080/24701556.2019.1711121
[41] Mousavi-Kouhi SM, Beyk-Khormizi A, Amiri MS, et al. Silver-zinc oxide nanocomposite: from synthesis to antimicrobial and anticancer properties. Ceram Int. 2021;47(15):21490–21497. doi: 10.1016/j.ceramint.2021.04.160
[42] Jin S-E, Jin H-E. Antimicrobial activity of zinc oxide nano/microparticles and their combinations against pathogenic microorganisms for biomedical applications: from physicochemical characteristics to pharmacological aspects. Nanomaterials. 2021;11(2):263. doi: 10.3390/nano11020263
[43] Pino P, Bosco F, Mollea C, et al. Antimicrobial nano-zinc oxide biocomposites for wound healing applications: a review. Pharmaceutics. 2023;15(3):970. doi: 10.3390/pharmaceutics15030970
[44] Dixit A, Sabnis A, Shetty A. Antimicrobial edible films and coatings based on N,O-Carboxymethyl chitosan incorporated with Ferula Asafoetida (Hing) and Adhatoda Vasica (Adulsa) extract. Adv Mater Process Technol. 2022;8(3):2699–2715. doi: 10.1080/2374068X.2021.1939982
[45] Jain D, Shivani, Bhojiya AA, et al. Microbial fabrication of zinc oxide nanoparticles and evaluation of their antimicrobial and photocatalytic properties. Front Chem. 2020;8:778. doi: 10.3389/fchem.2020.00778
[46] Lv X-H, Ren Z-L, Zhou B-G, et al. Discovery of N-(benzyloxy)-1, 3-diphenyl-1H-pyrazole-4-carboxamide derivatives as potential antiproliferative agents by inhibiting MEK. Bioorg Med Chem. 2016;24(19):4652–4659. doi: 10.1016/j.bmc.2016.08.002
[47] Reddy VG, Srinivasa Reddy T, Lakshma Nayak V, et al. Design, synthesis and biological evaluation of N-((1-benzyl-1H-1, 2, 3-triazol-4-yl) methyl)-1, 3-diphenyl-1H-pyrazole-4-carboxamides as CDK1/Cdc2 inhibitors. Eur J Med Chem. 2016;122:164–177. doi: 10.1016/j.ejmech.2016.06.011
[48] Wang S-F, Yin Y, Zhang Y-L, et al. Synthesis, biological evaluation and 3D-QSAR studies of novel 5-phenyl-1H-pyrazol cinnamamide derivatives as novel antitubulin agents. Eur J Med Chem. 2015;93:291–299. doi: 10.1016/j.ejmech.2015.02.018
[49] Zalewski P, Skibiński R, Talaczyńska A, et al. Stability studies of cefoselis sulfate in the solid state. J Pharm Biomed Anal. 2015;114:222–226. doi: 10.1016/j.jpba.2015.05.033
[50] Vaarla K, Kesharwani RK, Santosh K, et al. Synthesis, biological activity evaluation and molecular docking studies of novel coumarin substituted thiazolyl-3-aryl-pyrazole-4-carbaldehydes. Bioorganic Med Chem Lett. 2015;25(24):5797–5803. doi: 10.1016/j.bmcl.2015.10.042
[51] Nayak N, Ramprasad J, Dalimba U. Synthesis and antitubercular and antibacterial activity of some active fluorine containing quinoline–pyrazole hybrid derivatives. J Fluor Chem. 2016;183:59–68. doi: 10.1016/j.jfluchem.2016.01.011

[52] Khloya P, Kumar S, Kaushik P, et al. Synthesis and biological evaluation of pyrazolylthiazole carboxylic acids as potent anti-inflammatory–antimicrobial agents. Bioorganic Med Chem Lett. 2015;25(6):1177–1181. doi: 10.1016/j.bmcl.2015.02.004

[53] Miniyar PB, Barmade MA, Mahajan AA. Synthesis and biological evaluation of 1-(5-(2-chloroquinolin-3-yl)-3-phenyl-1H-pyrazol-1-yl) ethanone derivatives as potential antimicrobial agents. J Saudi Chem Soc. 2015;19(6):655–660. doi: 10.1016/j.jscs.2013.12.004

[54] Viveka S, Shama P, Nagaraja GK., et al. Design and synthesis of some new pyrazolyl-pyrazolines as potential anti-inflammatory, analgesic and antibacterial agents. Eur J Med Chem. 2015;101:442–451. doi: 10.1016/j.ejmech.2015.07.002

[55] Abdellatif KR, Elshemy HA, Azoz AA. 1-(4-methane (amino) sulfonylphenyl)-3-(4-substituted-phenyl)-5-(4-trifluoromethylphenyl)-1H-2-pyrazolines/pyrazoles as potential anti-inflammatory agents. Bioorg Chem. 2015;63:13–23. doi: 10.1016/j.bioorg.2015.09.002

[56] Kumar H, Bansal KK, Goyal A. Synthetic methods and antimicrobial perspective of pyrazole derivatives: an insight. Anti-Infective Agents. 2020;18(3):207–223. doi: 10.2174/2211352517666191022103831

[57] Marinescu M. Synthesis of antimicrobial benzimidazole–pyrazole compounds and their biological activities. Antibiotics. 2021;10(8):1002. doi: 10.3390/antibiotics10081002

[58] Alnufaie R, Raj KC H, Alsup N, et al. Synthesis and antimicrobial studies of coumarin-substituted pyrazole derivatives as potent anti-staphylococcus aureus agents. Molecules. 2020;25(12):2758. doi: 10.3390/molecules25122758

[59] Elfahham HA, Elgemeie GEH, Ibraheim YR, et al. Studies on 3, 5-diaminopyrazoles: new routes for the synthesis of new pyrazoloazines and pyrazoloazoles. Liebigs Ann Chem. 1988;1988(8):819–822. doi: 10.1002/jlac.198819880820

[60] Kryštof V, Cankař P, Fryšová I, et al. 4-arylazo-3, 5-diamino-1 H-pyrazole CDK inhibitors: SAR study, crystal structure in complex with CDK2, selectivity, and cellular effects. J Med Chem. 2006;49(22):6500–6509. doi: 10.1021/jm0605740

[61] Karcı F, Demirçalı A. Synthesis of disazo pyrazolo [1, 5-a] pyrimidines. Dyes Pigments. 2007;74(2):288–297. doi: 10.1016/j.dyepig.2006.02.007

[62] Srinivasan D, Nathan S, Suresh T, et al. Antimicrobial activity of certain Indian medicinal plants used in folkloric medicine. J Ethnopharmacol. 2001;74(3):217–220. doi: 10.1016/S0378-8741(00)00345-7

[63] William H. Microbiological assay, an introduction to quantitative principles and evaluation. New York: Academic Press; 1977.

[64] Ge B, Wang F, Sjölund-Karlsson M, et al. Antimicrobial resistance in campylobacter: susceptibility testing methods and resistance trends. J Microbiol Methods. 2013;95(1):57–67. doi: 10.1016/j.mimet.2013.06.021

[65] Turan N, Kaya E, Gündüz B, et al. Synthesis, characterization of poly (E)-3-amino-4-((3-bromophenyl) diazenyl)-1H-pyrazol-5-ol: investigation of antibacterial activity, fluorescence, and optical properties. Fibers Polym. 2012;13(4):415–424. doi: 10.1007/s12221-012-0415-2

[66] Sharma D, Sabela MI, Kanchi S, et al. Biosynthesis of ZnO nanoparticles using jacaranda mimosifolia flowers extract: synergistic antibacterial activity and molecular simulated facet specific adsorption studies. J Photochem Photobiol, B. 2016;162:199–207. doi: 10.1016/j.jphotobiol.2016.06.043

[67] Bharathi D, Bhuvaneshwari V. Synthesis of zinc oxide nanoparticles (ZnO NPs) using pure bioflavonoid rutin and their biomedical applications: antibacterial, antioxidant and cytotoxic activities. Res Chem Intermed. 2019;45(4):2065–2078. doi: 10.1007/s11164-018-03717-9

[68] Vanathi P, Rajiv P, Narendhran S, et al. Biosynthesis and characterization of phyto mediated zinc oxide nanoparticles: a green chemistry approach. Materials Letters. 2014;134:13–15. doi: 10.1016/j.matlet.2014.07.029